JOURNAL OF AIRCRAFT
Vol. 42, No. 1, January–February 2005

Huygens Structure Atmospheric Instrument 2002 Balloon Campaign: Probe–Parachute System Attitude Analysis

V. Gaborit*
LESIA, Observatory of Paris–Meudon, 92195 Meudon, France
M. Antonello† and G. Colombatti‡
University of Padua, 1 35131 Padua, Italy
and
M. Fulchignoni§
Université Denis Diderot/LESIA, Observatory of Paris–Meudon, 92195 Meudon, France

The results of the attitude analysis during the descent phase of the 2002 Huygens Structure Atmospheric Instrument balloon test are presented. The data of three instruments (magnetometer, accelerometer and tilt sensor) are analyzed. Magnetometer data are useful to characterize the probe-parachute system pendulum and spinning motions. The tilt angle descent profile is derived and shows a very strong pendulum motion just after probe release. The initial tilt angle is about 40 deg and damps slowly during the first 500 s of the descent phase. This tilt angle profile is compared with the one derived using accelerometer data. The quite good agreement obtained between the two profiles is very important in anticipation for the Huygens mission. The determination of the tilt angle using two different methods provides the opportunity to better understand tilt sensor data. The tilt sensor is able to detect pendulum motions with short periods (about 2 s) but seems not suitable for periods greater than 12 s. This is important for the Huygens mission because the period of the pendulum motion should reach at least 17 s. Finally, the experimental probe spin profile is reconstructed and appears very different from the one expected.

Introduction

ON 30 May 2002, the Huygens Atmospheric Structure Instrument (HASI) team performed a successful balloon flight.[1,2] A 1:1 scaled mock-up of the Huygens probe was lifted up to an altitude of 32.5 km by means of a stratospheric balloon, then released after a floating phase, and decelerated by an Irvin-supplied, hemispherical-shape parachute. The main goals of this flight were 1) to test the spare sensors of the HASI experiment onboard Huygens[3] in dynamic conditions, 2) to exercise the trajectory reconstruction algorithm[4] in anticipation of the real Huygens mission, and 3) to investigate the probe–parachute system motion throughout the descent.

The Huygens probe mock-up consists of four parts: a gondola, a ring supporting a double-plate platform, a bottom front cone, and an upper cover (Fig. 1). Spin vanes are fixed on the gondola to provide a spin rate similar to the one expected for the real Huygens mission. The HASI experiment comprises four accelerometers (an axial Xservo and a three-axis X, Y, Z piezo), two redundant temperature sensor units, and a pressure sensor. To investigate the dynamic behavior of the probe–parachute system during the descent phase, several sensors were added on the probe's platform (Fig. 2), including the spare tilt sensor of the Huygens' Surface Science Package (SSP) (see Ref. 5), a three-axis magnetometer, and two sun sensors.

The descent flight chain comprises (Fig. 3) 1) the probe with all of the instruments and a personal computer for onboard data storage, 2) a telemetry (TM) box located about 2.6 m above the probe, and 3) a hemispherical Irvin-supplied parachute linked to the TM by means of a heavy bifilar line supporting all of the devices to perform the probe release.

The mass of the different elements are 168, 124, and 156 kg for the probe, the TM box, and the parachute (with the bifilar line), respectively. Data were successfully acquired during the ascent and the floating and descent phases: 100% of the data were recovered on the hard disk.

The aim of this paper is to determine the attitude of the probe–parachute system (tilt angle and spin rate) during the descent phase and to report on the methods used. Magnetometer data are analyzed to retrieve the tilt angle throughout the descent and to see what information about the probe attitude can be extracted from the accelerometer and SSP–tilt sensor data. The characteristics of the three instruments are given in Table 1. Then, the choice of the spin vane cascade parameters is described and the experimental spin rate profile is discussed.

Pendulum Motion

Tilt Angle Determination Through Magnetometer Data Analysis

The magnetometer is a commercial triaxial fluxgate magnetometer (mag-03MS100, Bartington Instruments) (Table 1). It measures the components of the magnetic field inside the probe: M_X, axial component and M_Y and M_Z, transverse components, during both the ascent and the descent phase. During the whole flight, the magnetometer measures the sum of two fields: the Earth magnetic field and an additional internal magnetic field induced by the probe electronics. Consequently, to retrieve informations about the probe attitude, it is necessary to correct measurements from this additional internal magnetic field. This correction was determined during the ascent phase, during which the probe plane remains quasi-horizontal.

Analyzing M_Y and M_Z data by representing M_Z with respect to M_Y (Fig. 4a), we see that the additional internal magnetic field is significant and that it depends on the probe's orientation (with respect to the Earth magnetic field). The quadratic form $M_Z = f(M_Y)$, which should be represented by a circle (if the probe plane is horizontal) is represented by an ellipse rotated with respect to the M_Y and M_Z axes. This means that the magnetic field induced by the probe electronics changes the phase (which is not 90 deg anymore) between

Received 25 August 2003; revision received 27 January 2004; accepted for publication 27 January 2004.

*Doctor, Pôle Planetologie, Table Équatoriale, 5 Place Jules Janssen.
†Doctor, Centro Interdipartimentale Studi ed Attività Spaziali "G. Colombo," via Venezia.
‡Doctor, Centro Interdipartimentale Studi ed Attività Spaziali "G. Colombo," via Venezia.
§Professor, Pôle Planetologie, Bâtiment 10, 5 Place Jules Janssen.

M_y and M_z measurements. Consequently, analyzing the quadratic form $M_Z = f(M_Y)$, we were able to extract the contribution of the Earth magnetic field from M_Y and M_Z data.

This contribution is represented in Fig. 4a by the circular shape, which is shifted with respect to the center ($M_Y = 0$, $M_Z = 0$). This shift results from the (M_Y, M_Z) plane being slightly inclinated with respect to the horizontal plane. This can be observed in Fig. 4b, where the probe axial component M_X and the probe transverse component $\sqrt{(M_Y^2 + M_Z^2)}$ are represented. The obtained curves are exactly in phase opposition, and the amplitude of the oscillations are very consistant with 1) a magnetic dip angle i of about -54 deg and 2) an inclination of the (M_Y, M_Z) plane with respect to the horizontal of about 5.5 deg. Consequently, we deduced that the M_X component was not (or was very weakly) affected by the additional internal magnetic field.

Finally, we were able to retrieve the Earth magnetic field accurately (Fig. 5).

The properties of the measured Earth magnetic field are summarized in Table 2 for two different altitudes that correspond to the beginning and the end of the ascent phase.

The method used to recover the Earth magnetic field was applied for the whole flight. This method is less accurate at the beginning of the descent ($12{,}954 < t < 14{,}000$ s) because of the strong pendulum motion of the probe–parachute system, as we will see later. As seen in Table 2, the internal magnetic field depends on the orientation of the probe. Consequently, the correction of the M_Y and M_Z components, calculated when the probe's plane is horizontal, is not adequate for this part of the descent. Hopefully, our determination of the tilt motion of the probe–parachute system during the descent phase will require only the following:

1) M_X data that are not affected by this internal magnetic field may be required. These data are presented in Fig. 6a.

2) The Earth magnetic field's profile, which is accurately determined during the ascent phase, may be required.

Performing a Fourier analysis on M_X data, we observe that the signal can be decomposed into two components (Fig. 6b). The main component (dotted line) shows oscillations with a period between $\sim$12 s at the beginning of the descent and $\sim$20 s, 400 s after the probe release. These values for the oscillation period are of the same order as the theoretical period of 17 s derived from the simple pendulum formula. Thus, this main component extracted from M_X data seems to be driven by the global probe–parachute system pendulum motion. The second component (solid line) shows a periodic signal, with a mean period of 2 s, corresponding to the theoretical period obtained when a pendulum motion of the probe is considered with respect to the TM box. The straps linking the probe and the TM box have a length of 1.2 m. The maximum amplitude is reached at $t \simeq 150$ s. The signal is also modulated in amplitude, showing

Fig. 1 Integrated mock-up with its different elements (gondola, ring, cone, and upper cover).

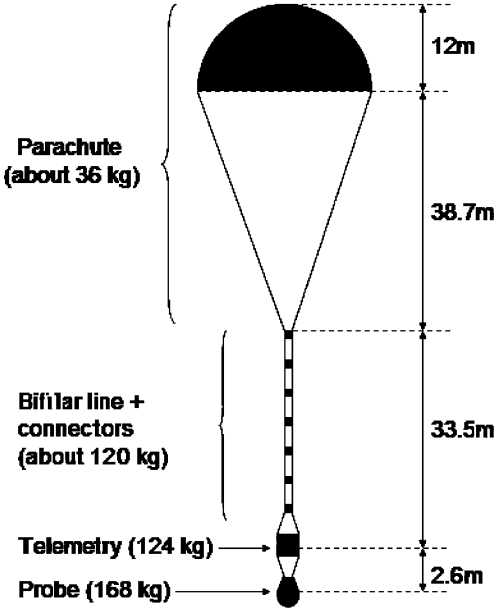

Fig. 3 Schematic of the descent flight chain.

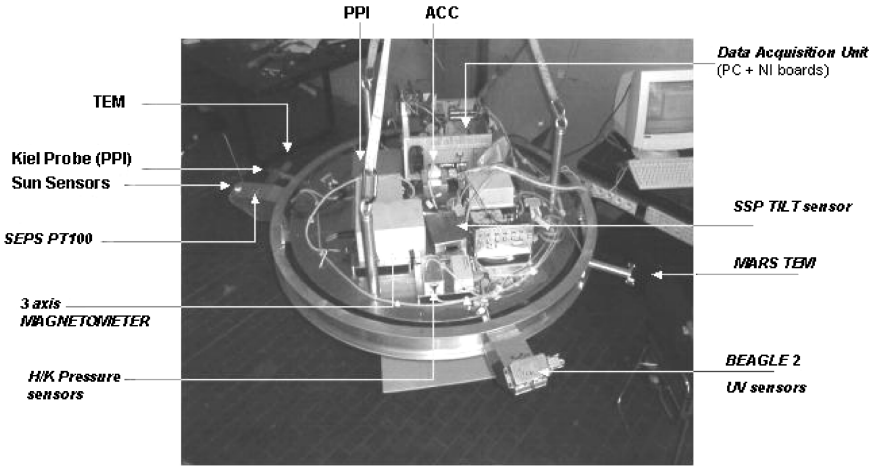

Fig. 2 Platform of the probe with all of the instrumentation.

Table 1 Sensor characteristics

Instruments	Range	Accuracy	Resolution	Alignment error between axes	Offset error
Accelerometer (Xservo)	0–15 g[a]	<150 mg (1% OFS[b])	7 mg	——	$<\pm 10$ mg
Magnetometer (each axis)	0–100 μT	± 0.5 % (OFS)	50 nT	<0.1 deg	± 5 nT
SSP–tilt (each axis)	0–90 deg	± 0.5 deg	0.07 deg	<0.1 deg	$<\pm 0.1$ deg

[a] $g = 9.81\ \mathrm{m \cdot s^{-2}}$. [b] OFS, of full scale.

Table 2 Mesured properties of the Earth magnetic field vs altitude

Magnetic field	0 km	32.5 km
B_h, μT (horizontal)	25.8 ± 1.0	25.8 ± 1.0
B_z, μT (vertical)[a]	35.9 ± 0.5	35.1 ± 0.5
B, μT (modulus)	44.2 ± 1.0	43.5 ± 1.0
i, deg (dip angle)	54.3 deg $\pm$ 1.4 deg	53.7 deg $\pm$ 1.4 deg

[a] Vertical gradient is approximately $-21.5\ \mathrm{nT \cdot km^{-1}}$, close to the theoretical value of $-20.9\ \mathrm{nT \cdot km^{-1}}$ calculated from the formula $\mathrm{d}B/\mathrm{d}r = -(3B/r)$, where r is the distance from the center of the modeled magnetic dipole, that is, considered here as the center of the Earth.

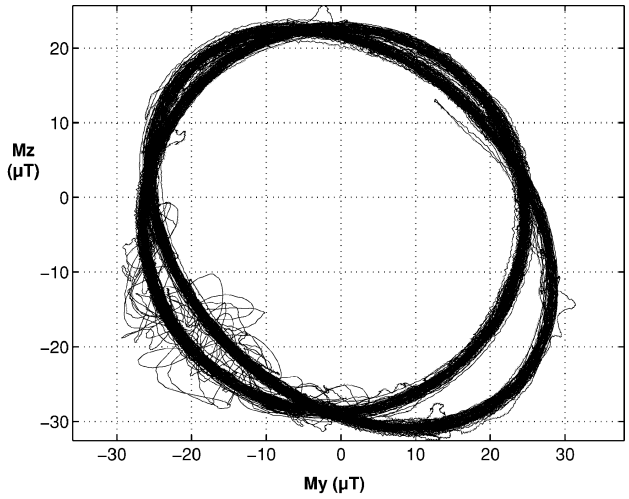

Fig. 4a M_Z vs M_Y before (elliptical shape) and after (cicular shape) correction of the additional internal magnetic field.

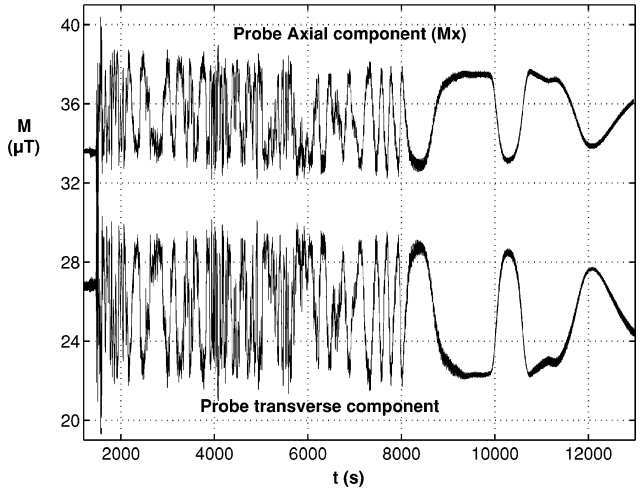

Fig. 4b Axial (M_X) and transverse [$\sqrt{(M_Y^2 + M_Z^2)}$] component of the Earth magnetic field vs time during the ascent phase.

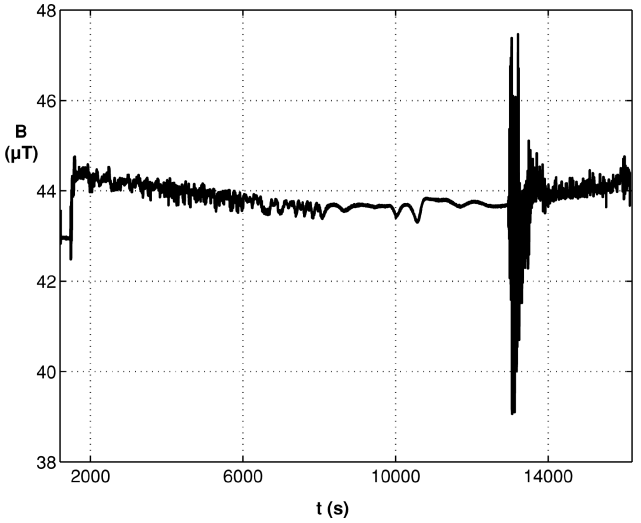

Fig. 5 Earth magnetic field B in microtesla vs time in seconds during the whole flight.

maxima and minima appearing with the same frequency as the one observed for the global pendulum motion. Then, it characterizes a complex double pendulum motion. However, in the following, we will assume that the pendulum motion of the probe with respect to the TM box is negligible.

To determine the tilt motion of the probe–parachute system, we consider the model with two-degree-of-freedom (2-DOF) θ and φ, shown in Fig. 7. Here, θ represents the angle between the probe–parachute axis and the vertical axis. The angle φ describes the coning motion and is defined with respect to the horizontal component of the Earth magnetic field. We will not take into account any spin rate here because M_X measurements are independant of any rotation around the probe–parachute axis.

The probe–parachute system is considered as a single pendulum with the following caracteristics:

1) The attachment point is the center of pressure. We assume that it is located at the center of the canopy mouth.

2) The loaded mass is the total mass of the probe, the TM, and the bifilar line. We assume that it is located at the center of gravity of those three masses, or about 68.8 m under the center of pressure.

With the data obtained during the flight, it would be impossible to describe a complex elliptical motion. In addition, accelerometer data suggest a coning or a weakly elliptical motion rather than a strongly elliptical motion. Consequently, we will assume in our model that the angle φ varies much faster than the tilt angle θ.

With all of the assumptions made, the evolution of M_X is given by Eq. (1):

$$M_X = \sin(\theta)\cos(\varphi)B_y + \cos(\theta)B_z \tag{1}$$

where B_y and B_z are, respectively, the horizontal and vertical components of the Earth's magnetic field. Because it is impossible to know the value of φ during the descent, the only point where we can derive the tilt angle θ is for $\varphi = 0[\pi]$. In fact, if θ

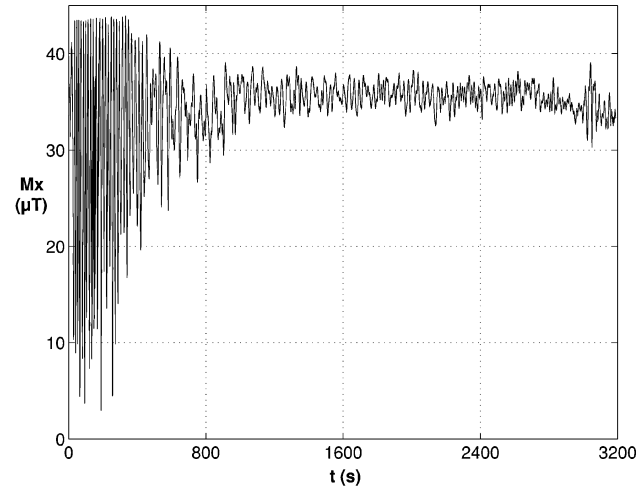

Fig. 6a M_X data used for attitude reconstruction.

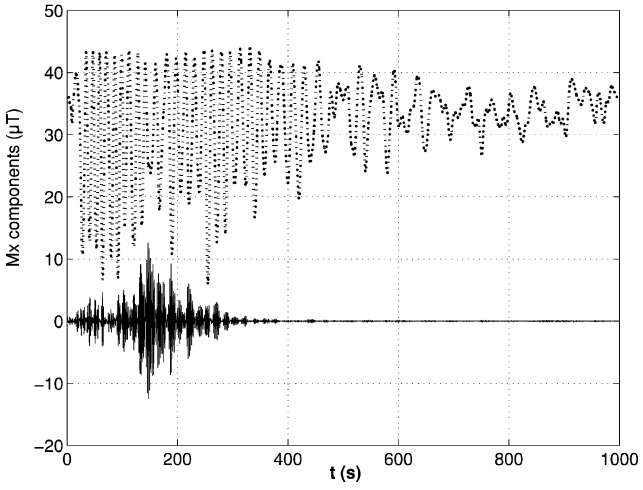

Fig. 6b Fourier decomposition of the M_X signal into two components: · · · ·, main component and ——, second component.

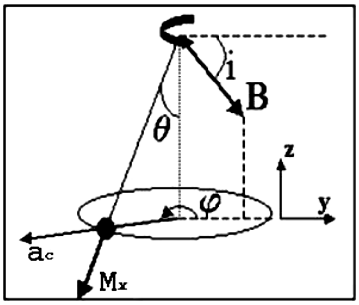

Fig. 7 Model for a 2-DOF pendulum motion.

varies slowly, that is, remains almost constant during one precession around the vertical axis, M_X is minimum for $\varphi = \pi$ and maximum for $\varphi = 0$.

Thus, by the use of each extremum of the M_X signal, it is possible to estimate the tilt angle of the probe–parachute system during the descent. The obtained values for the tilt angle are shown in Fig. 8. The angle θ increases quickly just after probe release to reach the value of about 36 deg after 30 s and the maximum value of 41 deg a bit later. This strong pendulum motion can be explained by the presence of horizontal winds acting on the parachute. The significant mass of the parachute, its large size, and the relatively small weight of the payload, that is, probe and TM, can also explain such a tilt angle.

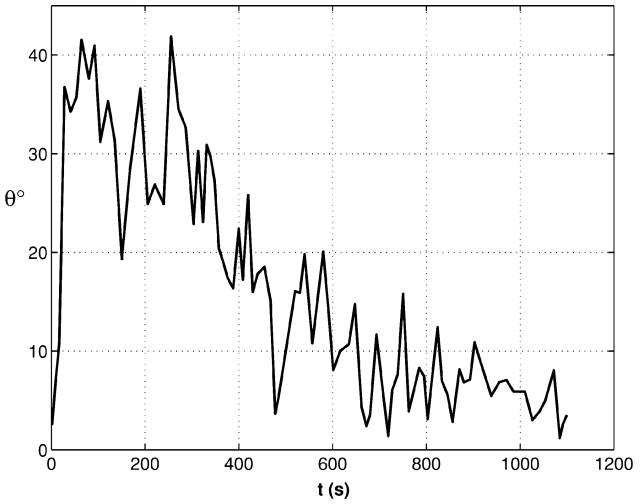

Fig. 8 Evolution of the tilt angle θ (in degrees) vs time during the nonstabilized part of the descent.

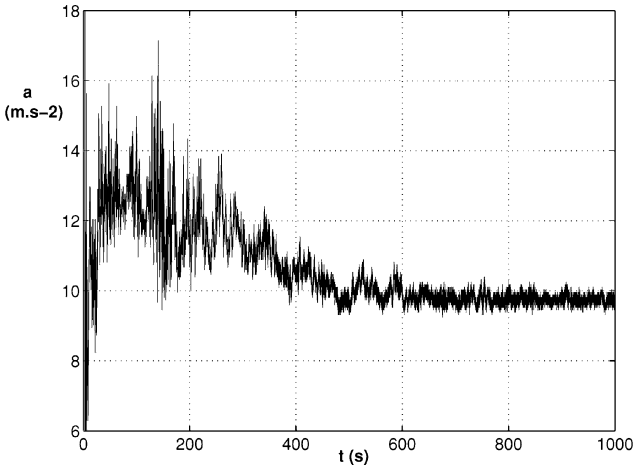

Fig. 9 Acceleration measured by the Xservo accelerometer (in $\mathrm{m \cdot s^{-2}}$) vs time (in seconds).

Subsequently, θ decreases slowly, with a duration of almost 1000 s. This slow decrease is explained by a very weak damping due to the low density at the corresponding altitude and by the presence of zonal winds and wind gusts that maintain the pendulum motion.

Xservo Data Interpretation

Measurements of the Xservo accelerometer are presented Fig. 9. During approximately the first 400 s, the measured acceleration always remains greater than g, and the observed difference between these measurements and g can not be explained if we consider only the aerodynamic deceleration due to the parachute. Only the pendulum motion can explain it, and this pendulum motion must resemble a coning motion. In fact, if the motion were strongly elliptical, the measured acceleration would vary rapidly between two extremum values: a value close to g (θ maximum) and a value much greater than g (θ minimum). Consequently, we will show that a coning motion can explain this acceleration profile.

The Xservo accelerometer is sensitive to the aerodynamic drag and to inertial forces. However, analyzing the descent velocity profile (next section), we see that aerodynamic deceleration is at a maximum of 30 s after probe release and equal to about $g + 0.2\ \mathrm{m \cdot s^{-1}}$. It then decreases asymptotically to reach g. Consequently, we will assume that the surplus of acceleration with respect to g is a consequence of the inertial forces induced by the pendulum motion of the probe–parachute system.

The axial component of the centrifugal acceleration a_{cX}, due to the pendulum motion, can be derived from the following equation:

$$a_{cX} = \omega^2 \times L \times \sin^2(\theta) \tag{2}$$

where $\omega = \mathrm{d}\varphi/\mathrm{d}t = \sqrt{(g/L\cos\theta)}$ is obtained under the assumption that the centrifugal acceleration balances the probe weight. L is the length of the probe–parachute system, that is, 70 m. Using the expressions of a_{cX} and ω, we find that the acceleration measured by the Xservo accelerometer should be given by the very simple equation:

$$a_{\mathrm{meas}} = g/\cos\theta \tag{3}$$

Figure 10a shows the comparison between Xservo data and those derived from Eq. (3) by the use of θ values as shown in Fig. 8. The good agreement between the model and experimental data shows that the acceleration profile can be explained by the 2-DOF model of the pendulum motion. In addition, it shows that it is possible to recover the tilt angle, by the use of acceleration measurements, by inversion of Eq. (3). The result of this inversion is plotted in Fig. 10b. Tilt angle values derived from Xservo measurements and from M_X data are consistent, but differ a little for $30 < t < 50$ s, $120 < t < 150$ s, and $210 < t < 220$ s. In fact, if we refer to Fig. 6, the pendulum motion of the probe with respect to the TM box seems to be significant during these periods and slightly affect the tilt angle determination. When the tilt angle becomes smaller than 10 deg, the results are not as good because our model seems to reach its limits: For small tilt angles, the pendulum motion may have a large ellipticity, and, in this case, a circular approach is not valid anymore.

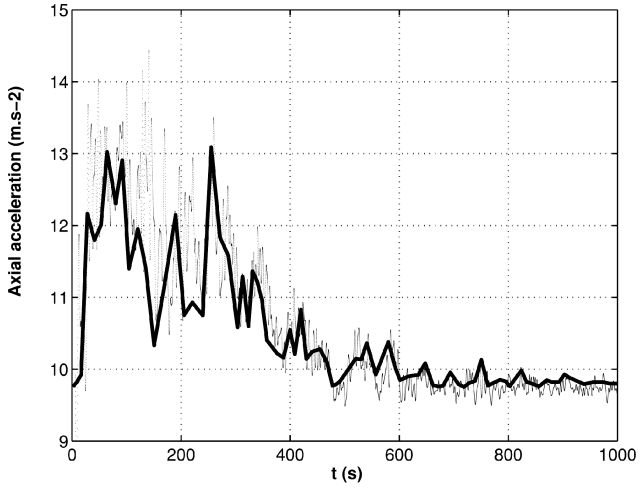

Fig. 10a X component of the acceleration (in $\mathrm{m \cdot s^{-2}}$) vs time (in seconds); comparison between Xservo data, —— and the acceleration profile, —— derived from the 2-DOF model.

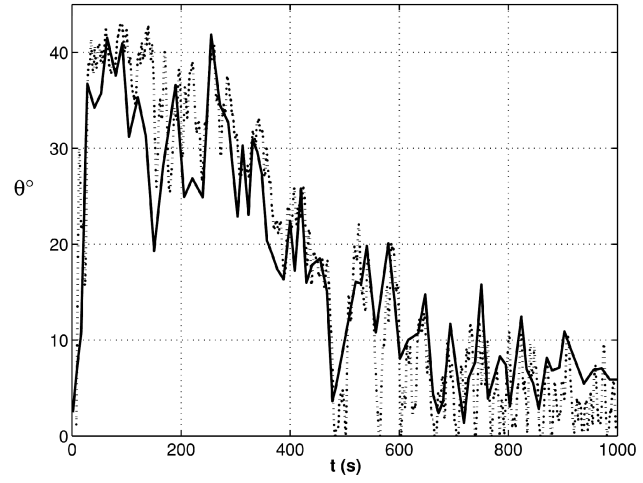

Fig. 10b Tilt angle (in degrees) vs time (in seconds); comparison between the tilt angle profiles derived from magnetometer data, —— and Xservo data · · · ·.

Finally, this tilt angle reconstruction shows that Xservo data should have a significant role for the attitude reconstruction during the real Huygens mission. This reconstruction should be easier because the flight chain for the Huygens mission is simpler, that is, no TM box, than the one used for this balloon flight. In addition, for the Huygens mission, the attitude reconstruction will have the benefit of other experiments sensitive to the attitude of the probe such as the Doppler wind experiment[6] and descent imager/spectral radiometer[7] experiments. However, the attitude reconstruction must be investigated further because the model developed in this study is not accurate enough, especially to describe small amplitude motions. It would also be of interest to include the effects of the added mass (air located under the canopy of the parachute) on the pendulum motion.

SSP–Tilt Sensor Analysis

The tilt sensor measures two angles, α_X and α_Y, defined as the angle between the X_{tilt} and the Y_{tilt} axes, respectively (located in the probe transverse plane), and the horizontal plane. The X_{tilt} and Y_{tilt} axes are perpendicular.

The principle of the measurement is to determine the displacement of a conductive fluid between two electrodes[5] induced by the pendulum motion of the probe–parachute system in a local gravity field. From the two angles α_X and α_Y, it is possible to retrieve the global tilt angle α, that is, between the probe plane and the horizontal plane, through the following formula:

$$\alpha = \arccos\sqrt{\cos^2(\alpha_x) - \sin^2(\alpha_y)} \tag{4}$$

Results for the global tilt angle α are represented in Fig. 11. The angle α is shown only for the first 1000 s of the descent. After 1000 s, α remains essentially constant. During the free-fall phase (which is barely visible on this graph), α increases very rapidly from 0 to 30 deg, but the measurements are not significant, given that the apparent gravity field equals zero during this phase. After the free-fall phase until about 300 s after probe release, the measured tilt angle remains less than 5 deg, and this maximum value is reached for $t \simeq 150$ s. From $t = 300$ s down to the ground, α maintains a constant value of about 1.2 deg, which seems to be the inclination of the probe plane with respect to the horizontal when the probe–parachute system is stabilized. This inclination is a result of the distribution of mass in the probe plane not being perfectly symmetrical. Then the probe plane is slightly tilted with respect to the horizontal.

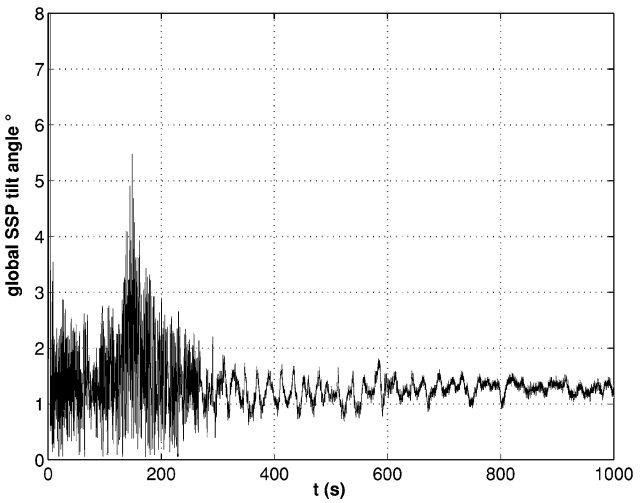

Fig. 11 Tilt angle derived from SSP–tilt sensor measurements (in deg) vs time (in seconds).

The tilt angle measured by the SSP–tilt sensor is very different than the one recovered from M_X or Xservo data. Nevertheless, the signal is very similar to the one characterizing the pendulum motion of the probe with respect to the TM box (observed in Fig. 6b), with the same period of 2 s, a maximum at around $t \simeq 150$ s and the same modulation in frequency. Thus, the SSP–tilt sensor seems to be sensitive only to short period oscillations and can not detect directly the global pendulum motion of the probe–parachute system.

With regard to the Huygens mission, the results should be similar because the length of the probe–parachute system will be only about 10 m during the SSP–tilt sensor operational phase (vs $L = 70$ m for our experiment), and the gravity field will be six times lower than the Earth's, leading to oscillations with a period of about 17 s, as for our experiment. Consequently, during the Huygens mission, the SSP–tilt sensor will be very useful to investigate the probe wobbling, but will probably not be the best instrument to characterize accurately the global pendulum motion.

Spin Analysis

The methodology adopted for the design of the mock-up spin vanes is now presented. The aerodynamic forces on the vanes have been evaluated with the theory of two-dimensional flow through cascade described by Scholz.[8] The final geometrical configuration of the axial cascade has been chosen to obtain the prescribed mission values of the spin velocity. The calculation has been simplified by the assumption of an instantaneous opening of the parachute.

Descent Velocity

The torque applied around the probe's spin axis depends on the descent vertical velocity. This vertical velocity is obtained through Equation (5),

$$m\frac{\mathrm{d}^2h}{\mathrm{d}t^2} = \frac{1}{2}\rho(h)\left(\frac{\mathrm{d}h}{\mathrm{d}t}\right)^2 (C_{rp}A_p + C_{rm}A_m) - mg \qquad (5)$$

where h is the probe altitude, m the total mass of the flight chain, ρ the atmospheric density, and g the local gravity field. $C_{rp} = 0.54$ and $C_{rm} = 0.75$. They are the specified parachute and the probe drag coefficients, respectively. $A_p = 452\ \mathrm{m}^2$ and $A_m = 1.34\ \mathrm{m}^2$; they are the corresponding reference areas. In Eq. (5), both the drag coefficients and the gravity field are assumed to be constants. The values of the drag coefficients are those measured for a zero value of the angle of attack. Because the floating altitude is about 32 km, g is considered constant equal to the standard value $g = 9.81\ \mathrm{m \cdot s^{-2}}$. The variation of ρ with the altitude is obtained through an exponential fitting of the U.S. Standard Atmosphere model data[9]: $\rho = 1.21 \times \exp(-2.12 \times 10^{-5} h^{1.18})$.

In Fig. 12a, the measured values of the density are compared with those calculated with Eq. (5): The agreement between the two sets of data is good. With this modeled density profile, Eq. (5) has been integrated by means of a fourth-order Runge–Kutta scheme. In Fig. 12b, the calculated vertical velocity profile (dashed line) is compared with the reconstructed one[4] during the 2002 balloon flight campaign. This calculated velocity is not in good agreement with the experimental profile. In fact, the velocity obtained 300 s after release achieves and remains higher than the approximately $2\ \mathrm{m \cdot s^{-1}}$ one observed and leads to a descent that lasts only 2550 s instead of 3188 s. These discrepancies can be due to vertical winds or errors in the given C_{rp} value. If we consider only vertical winds, they should blow upward with a mean amplitude of about $2\ \mathrm{m \cdot s^{-1}}$ from the lower troposphere up to an altitude of about 22 km (corresponding to the time $t = 300$ s).

If we derive the C_{rp} coefficient assuming negligible upward winds, we find that the C_{rp} coefficient should be given by the linearized relation: $C_{rp} = 0.925 - 0.0075 \times v_z$, where $v_z = \mathrm{d}h/\mathrm{d}t$. The curve in dotted-line [Fig. 12-(bottom)] shows the results of the integration performed with such a C_{rp} coefficient. This theoretical curve fits well with the experimental one and respects three important conditions: i) the maximum speed of $50\ \mathrm{m \cdot s^{-1}}$ obtained at $t = 17$ s, ii) the final speed of about $4.5\ \mathrm{m \cdot s^{-1}}$ at the end of the descent, and iii) the duration of the descent (i.e., 3188 s). But such variations of the C_{rp} coefficient seem not realistic for an hemispherical parachute. Consequently, we guess that the discrepancies between the real profile and the one derived with $C_{rp} = 0.54$ are mainly due to upward winds.

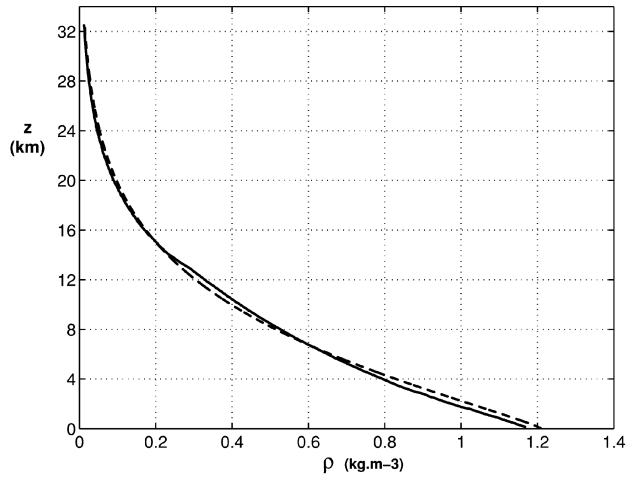

Fig. 12a Density (in kilograms per cubic meter) vs altitude (in kilometers): ——, experimental data and – – –, data obtained from the U.S. Standard Atmosphere model.[9]

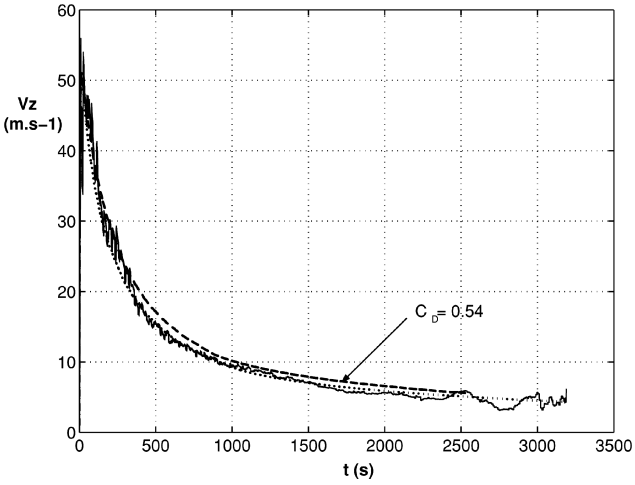

Fig. 12b Vertical velocity (in meters per seconds) vs time (in seconds): ——, experimental data; – – –, data obtained by integration of Eq. (5) with $C_{rp} = 0.54$; and · · ·, data obtained by integration of Eq. (5) with $C_{rp} = 0.925 - 0.0075 \times v_z$.

In the following subsection, the predicted spin rate profile was calculated (before the launch) with the C_{rp} value specified by the Irvin company, that is, $C_{rp} = 0.54$, and then the corresponding vertical velocity profile. This value tends to overestimate v_z or to overestimate the spin rate.

Spin Vane Configuration

Because the geometry of the blades is the same as used on the original probe, only the stagger angle γ and the number of vanes Z can be changed, so that the spin rate ω will accommodate the following constraints for the Huygens mission on Titan: $1 \leq \omega \leq 15$ rpm.

The axial torque M_z that induces the spin rate ω can be expressed as

$$M_z = [F_L \cos(\beta) - F_D \sin(\beta)] Z \bar{r} \qquad (6)$$

where F_L and F_D are, respectively, the lift and drag of the single blade of the cascade; $\bar{r}$ is the mean radial distance of the blades from the probe axis; and β is the angle between the freestream velocity and the normal to the cascade axis. After substitution of F_L

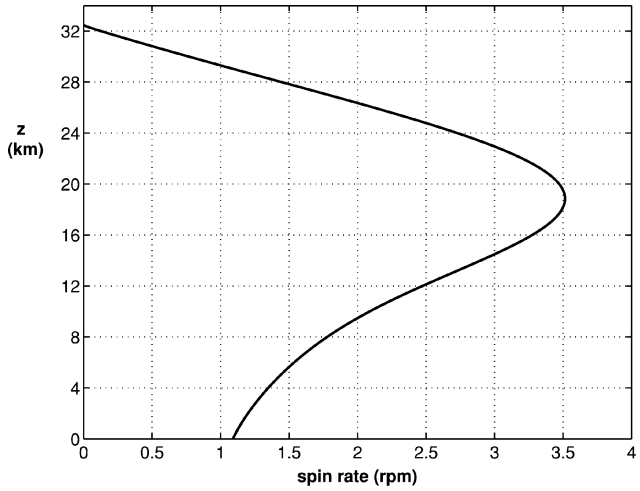

Fig. 13 Simulated spin rate profile (in revolutions per minute) vs altitude (in kilometers).

and F_D with the functionnal expression of the blade aerodynamic coefficients C_L and C_D of the blades in the cascade, Eq. (6) becomes

$$M_z = \tfrac{1}{2}\rho\left\{v_z^2 + [\omega\bar{r} + v_z\tan(\gamma)]^2/4\right\}^{0.5} \times [C_L v_z - 0.5C_D(\omega\bar{r} + v_z\tan\gamma)]Z\bar{r}\lambda b \quad (7)$$

Where λ and b are, respectively, the chord length and the radial height of the blades. The aerodynamics coefficients of the blades in the cascade can be expressed by the use of the corresponding flat plate coefficients C_L^* and C_D^*, defined as follows: $C_{L,D} = KC_{L,D}^* = K2\pi\sin(\gamma - \beta)$.

K is the coefficient of mutual interference of a flat plate in a cascade. The value of this coefficient depends on the value of $\bar{r}$, λ, and γ and is tabulated in Ref. 8. To account for the deflection of the flow downstream of the cascade in all of the preceding equations, the outlet velocity $v_z\tan(\gamma)$ must be replaced with $[2qv_z\tan(\gamma) + \omega\bar{r}(1-q)]/(1+q)$, where $q = [ZK\cos(\gamma)\lambda]/4\bar{r}$ is the deflection coefficient.

According to Moiij,[10] the drag coefficient can be expressed as $C_D = 0.005\sqrt{[(8\times10^6)/R_e]} + C_L^2\lambda/\pi b$, where R_e is the Reynolds number for a spin vane.

Finally, the spin rate ω was calculated by solution of both Eq. (5) and the following Euler equation for rotational motion,

$$I\frac{\mathrm{d}\omega}{\mathrm{d}t} = M_z - M_f \quad (8)$$

where I is the moment of inertia of the probe with respect to the probe–parachute axis, and M_f is the frictional torque due to the slip ring. After some numerical simulations of the probe descent by the use of Eqs. (5) and (8), the following configuration of the spin vanes has been chosen: $\gamma = 3$ deg and $Z = 28$.

In Fig. 13, the probe spin velocity profile, simulated with a mean tilt angle $\theta = 20$ deg and no horizontal wind is shown. This choice of such an angle roughly takes into account the interactions between the probe–parachute system and wind gusts or wind shear.

The inability to account properly for probe attitude effects and transversal wind effects are the main limitations of the preceding model. Both of these effects cause a deviation of the upstream flow from the axial direction. Therefore, the pressure distribution can vary considerably from one vane to the other. To obtain a more realistic prediction of the spin rate profile, a three-dimensional numerical simulation of the flow around the probe is needed. The flat-plate aerodynamic model just described gives an indication of the spin rate profile that provides a useful tool for the spin vane design.

Experimental Results

The experimental spin profile was recovered by the use of the components of the Earth's magnetic field, measured in the probe

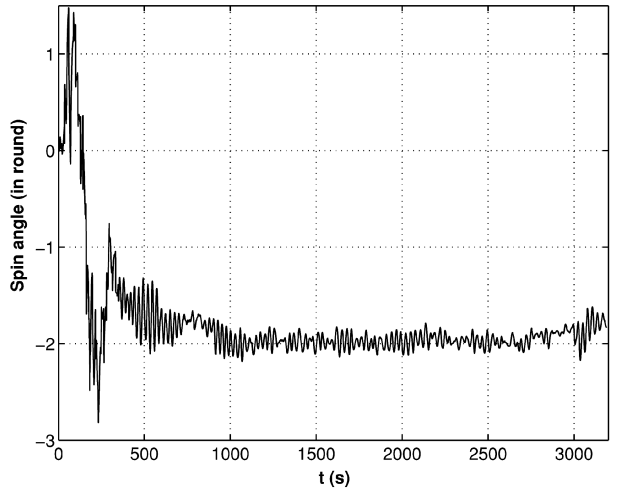

a)

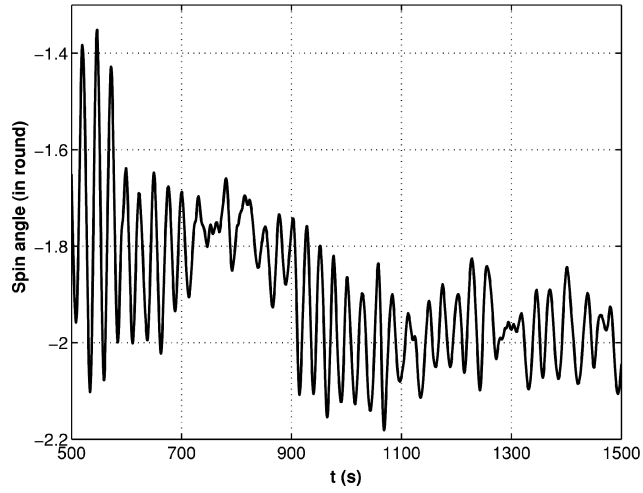

b)

Fig. 14 Experimental spin angle profile (in round) vs altitude (in kilometers); the spin angle is zero at the probe release: a) entire descent profile and b) an expansion of the data between $t = 500$ and 1500 s.

plane (M_Y and M_Z) and is given in Fig. 14a. As we saw in the third section, the corrections of M_Y and M_Z from the probe internal magnetic field are less accurate during the beginning of the descent because of the strong tilt motion of the probe–parachute system. That is why the reconstructed spin profile is very irregular at the beginning of the descent. This profile is very different from the expected one, the spin angle remaining almost constant throughout the descent with a mean spin rate close to zero. If the spin was dominated by the torque due to the presence of the spin vanes, then the spin rate should remain positive (positive rate for counterclockwise spinning) and the spin angle should increase continuously. As shown in Fig. 14b, this is not the case. After the period of strong pendulum motion, that is, $t > 500$ s, the spin angle oscillates around a mean and stable value, with a mean frequency of about 0.0374 Hz, that is, a 26.7 s-period.

This spin angle profile can be explained by the absence of a slip ring between the probe and the parachute and the presence of a nonsymmetric structure over the probe. In fact, throughout the descent, the airstream was able to cause a torque on the nonsymmetric structure, that is, the TM box, the bifilar line, and the parachute, and to prevent it from spinning. Because this structure was not separated from the probe by a slip ring and because the torque created by the spin vanes was not strong enough to impose the spinning on the whole structure, the probe was also prevented from spinning.

In conclusion, the retrieved spin rate profile is not as expected, but it is difficult to give any conclusion relative to the Huygens mission. In fact, on the one hand, the structure over the probe is very different

and much heavier than the one used for the real Huygens mission. On the other hand, the presence of a slip ring (used for the Huygens mission) between the probe and the upper structure appears to be crucial to retrieve a spin rate similar to the expected one.

Conclusions

We performed the reconstruction of the attitude profile during the descent phase of the 2002 HASI balloon test. Using the magnetometer and accelerometer data, we were able to recover independently two profiles that are in very good agreement. However, we need to improve our model to better characterize small-amplitude pendulum motions and a possible double pendulum motion. The reconstructed tilt angle profile shows that data from the Huygens SSP–tilt sensor are more likely to give information on wobbling (or on other fast oscillations of the probe) than on the global pendulum motion of the probe–parachute system. Finally, the spin angle profile was reconstructed, showing the very strong influence of the upper structure on the probe, and the importance of having a slip ring between them.

This work could help the descent trajectory working group and especially the attitude determination and reconstruction subgroup to define the relative significance of the different data sets for the Huygens probe attitude reconstruction.

To improve our understanding of parachute dynamics, a new HASI balloon flight is scheduled for summer 2003 and will include a gyroscope. It should allow us to reconstruct the attitude of the probe–parachute system in a more accurate manner and to optimize the results obtained with accelerometer data and SSP–tilt sensor data. In addition, the new flight chain included a slip ring to have exactly the same configuration as that of the Huygens mission, enabling further investigation of the influence of the pendulum motion on the spin rate.

References

[1]Fulchignoni, M., Aboudan, A., Angrilli, F., Antonello, M., Bastianello, S., Bettanini, C., Bianchini, G., Colombatti, G., Ferri, F., Flamini, E., Gaborit, V., Ghafoor, N., Hathi, B., Harri, A., Lehto, A., Lion Stoppato, P. F., Patel, M. R., and Zarnecki, J. C., "A Stratospheric Balloon Experiment to Test the Huygens Atmospheric Structure Instrument (HASI)," *Planetary and Space Sciences* (to be published, 2004).

[2]Bettanini, C., Fulchignoni, M., Angrilli, F., Lion Stoppato, P. F., Antonello, M., Bastianello, S., Bianchini, G., Colombatti, G., Ferri, F., Flamini, E., Gaborit, V., and Aboudan, A., "Sicily 2002 Balloon Campaign: A Test of the HASI Instrument," *Advances in Space Sciences* (to be published).

[3]Fulchignoni, M., Angrilli, F., Bianchini, G., Bar-Nun, A., Barucci, M. A., Borucki, W., Coradini, M., Coustenis, A., Ferri, F., Grard, R. J., Hamelin, M., Harri, A. M., Leppelmeier, G. W., Lopez-Moreno, J. J., McDonnell, J. A. M., McKay, C., Neubauer, F. H., Pedersen, A., Picardi, G., Pirronello, V., Pirjola, R., Rodrigo, R., Schwingenschuh, C., Seiff, A., Svedhem, H., Thrane, E., Vanzani, V., Visconti, G., and Zarnecki, J. C., "The Huygens Atmospheric Structure Instrument (HASI)," ESA SP 1177, 1997, pp. 163–176.

[4]Gaborit, V., Fulchignoni, M., Colombatti, G., Ferri, F., and Bettanini, C., "Huygens/HASI 2002 Balloon Test Campaign: Probe Trajectory and Atmospheric Vertical Profiles Reconstruction, *Planetary and Space Sciences* (to be published).

[5]Zarnecki, J. C., Banaszkiewicz, M., Bannister, M., Boynto, W. V., Challenor, P., Clark, B., Daniell, P. M., Delderfield, J., English, M. A., Fulchignoni, M., Garry, J. R. C., Geake, J. E., Green, S. F., Hathi, B., Jaroslawski, S., Leese, M. R., Lorenz, R. D., McDonnel, J. A. M., Merryweather-Clarke, N., Mill, C. S., Miller, R. J., Newton, G., Parker, D. J., Rabbetts, P., Svzdhem, H., Turner, R. F., and Wright, M. J., "The Huygens Surface Science Package," ESA SP 1177, 1997, pp. 177–195.

[6]Bird, M. K., Heyl, M., Allison, M., Asmar, S. W., Atkinson, D. H., Edenhofer, P., Plettemeier, D., Wohlmuth, R., Iess, L., and Tyler, G. L., "The Huygens Doppler Wind Experiment," ESA SP 1177, 1997, pp. 139–162.

[7]Tomasko, M. G., Doose, L. R., Smith, P. H., West, R. A., Soderblom, L. A., Combes, M., Bézard, B., Coustenis, A., de Berg, C., Lellouch, E., Rosenqvist, J., Saint-Pé, O., Schmitt, B., Keller, H. U., Thomas, N., and Gliem, F., "The Descent Imager/Spectral Radiometer (DISR) Aboard Huygens," ESA SP-1177, 1997, pp. 109–138.

[8]Scholz, N., "Aerodynamics of Cascade," AG-220, AGARD, 1977, pp. 212–220.

[9]NOAA-S/T76-1562, "U.S. Standard Atmosphere 1976," National Oceanagraphic and Atmospheric Administration, U.S. Government Printing Office, Washington, DC, 1976, p. 1277.

[10]Mooij, E., "ESA Huygens Probe and Descent Analysis," European Space Research and Technology Centre, ESTEC WP 1679, Oct. 1992.

[11]Atkinson, D. H., "Report of the Huygens Descent Trajectory Working Group," Technical Rept., Dept. of Electrical Engineering, Univ. of Idaho, Moscow, ID, June 1998.